RSC Advances

This is an *Accepted Manuscript*, which has been through the Royal Society of Chemistry peer review process and has been accepted for publication.

Accepted Manuscripts are published online shortly after acceptance, before technical editing, formatting and proof reading. Using this free service, authors can make their results available to the community, in citable form, before we publish the edited article. This *Accepted Manuscript* will be replaced by the edited, formatted and paginated article as soon as this is available.

You can find more information about *Accepted Manuscripts* in the Information for Authors.

Please note that technical editing may introduce minor changes to the text and/or graphics, which may alter content. The journal's standard Terms & Conditions and the Ethical guidelines still apply. In no event shall the Royal Society of Chemistry be held responsible for any errors or omissions in this *Accepted Manuscript* or any consequences arising from the use of any information it contains.

ROYAL SOCIETY OF CHEMISTRY

www.rsc.org/advances

A Two-step Method for Preparing $Li_4Ti_5O_{12}$-graphene as an Anode Material for Lithium-ion Hybrid Capacitors

Nansheng Xu, Xianzhong Sun, Xiong Zhang, Kai Wang, Yanwei Ma*

Key Laboratory of Applied Superconductivity, Institute of Electrical Engineering, Chinese Academy of Sciences, Beijing 100190, PR China

Abstract

Lithium-ion hybrid capacitors (LICs) are expected to fill the gap between the lithium-ion batteries and electrochemical supercapacitors. In this paper, we synthesize $Li_4Ti_5O_{12}$-graphene (LTO-G) by a two-step method and use it for the anode material in AC/LTO-G Li-ion hybrid capacitors. The LTO-G composite prepared by the two-step method shows the best electrochemical properties of the various ways, and it delivers a high specific capacity of 194 mAh g^{-1} at 0.1 C, and 90 mAh g^{-1} at 28.6 C. The AC/LTO-G capacitors can perform well between 1 and 2.5 V, and they deliver a reversible capacity of 80 mAh g^{-1} at 0.1 C. The energy density based on the total active material for these capacitors is 15 Wh kg^{-1} at 4000 W kg^{-1}, and 30 Wh kg^{-1} at 1000 W kg^{-1}. After 10,000 cycles, these capacitors still deliver an energy density higher than 22 Wh kg^{-1} at 1000 W kg^{-1}. The highest energy density based the total mass of the device is 6.6 Wh kg^{-1} and still have much room for improvement, which indicating that the LTO-G composite is a promising candidate anode material for Li-ion hybrid capacitors.

Keywords: Two-step method; Lithium ion hybrid capacitor; $Li_4Ti_5O_{12}$-Graphene; Anode.

* Corresponding author. Tel.: +86 10 82547129; fax: +86 10 82547137. E-mail address: ywma@mail.iee.ac.cn (Y. Ma).

RSC Advances Accepted Manuscript

1、Introduction

Lithium-ion hybrid supercapacitors (LICs) [1-16], which combine the high energy capacity of a lithium-ion battery and the rapid charge/discharge capability of a supercapacitor, are considered to be the second generation of supercapacitors [17] and are expected to fill the gap between the lithium-ion batteries and electrochemical capacitors [10, 11, 18]. Most LICs use the cathode materials of a lithium-ion battery (LIB) and activated carbon (AC) as the anode, or vice versa. The former devices, e.g., $LiFePO_4$/AC [13], $LiNi_{0.5}Mn_{1.5}O_4$/AC [14] and $LiCoO_2$/AC [15], deliver low cell voltage [9], and thus have a slightly better capacity than that of high voltage EDLCs. The other strategy is to develop high capacity supercapacitors using an AC cathode, while the anode materials of LIB for anode, e.g., AC/graphite [3, 19-21], AC/hard-carbon [8, 22], AC/Fe_2O_3 [9], and AC/TiO_2 [10], AC/$Li_4Ti_5O_{12}$ [5, 23-27]. Although Fe_2O_3 and other transition metal oxides deliver very high specific capacities, they suffer from large volume expansion during charge/discharge processes, which may cause the electrode material to pulverize and decrease its capacity [28]. Fe_2O_3 and other transition metal oxides are also undesirable for electrodes because they form Li_2O and therefore have a low first cycle coulombic efficiency [16, 29-31]. The formation of Li_2O is unfavorable for LICs, because it consumes the Li-ion of the electrolyte and which decreases the capacity.

Spinel $Li_4Ti_5O_{12}$ (LTO) was considered as one of the most promising anode materials for LIBs and LICs due to its unique properties including zero structure change and high and flat operating potential (1.55 V vs. Li^+/Li) during Li-ion insertion/extraction [1, 2, 5, 24, 32-36]. However, the slow Li^+ ion diffusion coefficient and

RSC Advances Accepted Manuscript

poor electron conductivity [24] prevents the LTO material from wide usage in high performance power systems. Reducing the particle size of LTO can significantly reduce the Li^+ ion diffusion path and rapidly increase the electrode reaction kinetic process [5, 28]. However, the nanosized LTO particles are hard to synthesize, and underproduced [5, 25, 37, 38]. The citric acid-nitrate combustion method [28] is an easy way to produce the very fine LTO precursor, but it needs further heat treatment to produce single phase LTO at an elevated temperature, for example 800 ^oC, which unfortunately causes the LTO particle to increase in size.

On the other hand, the electric conductivity can be increased to an extremely high level by adding conductive additives, e.g., carbon-coating [35, 39, 40], graphene [4, 32, 41], and carbon nanotubes [5, 42]. Among them, graphene, a two-dimensional (2D) honeycomb lattice exfoliated from graphite, was considered as the ideal conductive additive for hybrid nanostructured electrodes [41, 43-45], and it was widely used in energy technologies [4, 11, 31, 32, 41, 46-53]. The addition of graphene also helps to increase the electrochemical performance by increasing its specific capacity [4, 31, 43]. However，graphene is even hard to synthesize.

In this work, $Li_4Ti_5O_{12}$-Graphene (LTO-G) composite was synthesized through a two-step method, and its phase structure, particle morphology, and electrochemical properties were characterized. Two three-electrode systems, using AC as the cathode, LTO-G as the anode, and a lithium metal as a reference electrode, were assembled and studied.

2、Experimental

RSC Advances Accepted Manuscript

2.1. Synthesis

$Li_4Ti_5O_{12}$-Graphene (LTO-G) composite was prepared by a two-step method. First, $Li_4Ti_5O_{12}$ intermediate (denote as p-LTO) was synthesized by the combination of sol gel and citric acid-nitrate using the low temperature self-propagating combustion method [28], by according to the following steps. First, 0.125 mol $Ti(C_4H_9O)_4$ (Sinopharm Chemical Reagent Co., Ltd, SCRC) was dispersed in an 200 mL ethanol (solution A), and 0.11 mol $LiCH_3COO{\cdot}H_2O$ (from SCRC, $n_{Li}:n_{Ti} = 4.4:5$) was dispersed in 800 mL distilled water (solution B). 0.47 mol citric acid ($n_{\text{citric acid}}:n_{\text{total metal ion}} = 2:1$) and 50 mL nitric acid were added to solution B to obtain solution C. Ammonia (~28%) was added to adjust the pH of the solution C to approximately 6. The resultant solution was treated in an air-circulating oven at 80 °C to vaporize the water completely. The product was heat-treated in the oven at 200 °C for 2 h to cause combustion. The obtained precursor was ground and calcined in air at 650 °C for 4 h to obtain the p-LTO (treated at 800 °C for pure LTO).

Graphite oxide was used as the source for graphene, and was prepared by the conventional Hummers method. Briefly, 5 g graphite (SCRC) and 5 g sodium nitrate were added to 115 mL concentrated H_2SO_4. The mixed solution was placed in an ice-water bath and stirred for 4 h. 30 g $KMnO_4$ was then gradually added into the solution and stirred for another 4 h at room temperature. 230 mL distilled water was added slowly to quickly increase the temperature to 98 ^oC, and this temperature was held for 15 min. The suspension was then further diluted with 460 mL warm distilled

RSC Advances Accepted Manuscript

water and treated with 3% H_2O_2. The resulting suspension was washed and centrifuged several times to produce the graphite oxide solution.

Certain amount of the GO solution (the mass of GO is about 0.2 g) was diluted with 300 mL distilled water and treated with ultrasonic for 30 min. 0.9 g p-LTO was added to the GO solution, further treated with ultrasonic for another 30 min, and then transferred to a rotary evaporator and dried at 75 ^{o}C. After drying, the obtained powders (denote as p-LTO/GO) were well ground and then reduced at 800 ^{o}C in flowing Ar for 2 h to obtain the LTO-G composite (as described in Fig. 1). In order to make a comparison, the LTO-G composites prepared by these different methods were also investigated. In method I, the LTO-G was prepared by directly mixing the pure LTO and graphene together in the electrode preparation process. In method II, LTO-G was in-situ reduced from GO coated LTO at 500 ^{o}C in Ar for 1 h, as presented in Fig. 1.

In the two-step method, two intermediates, p-LTO and GO, were first prepared and then further heat-treated to synthesize the LTO-G composite after they were well mixed. Since the two-step method prepared LTO-G was first heat-treated at a lower temperature, it produced a finer powder. The GO coating layer will also prevented the p-LTO powders from aggregation and thus prevented the particle size of LTO from increasing during the heat treatment at 800 ^{o}C.

2.2. Characterization

The crystal structures of LTO-G powders were characterized by X-ray powder diffraction (XRD) using a Bruker D8 Advance Spectrometer with a Cu-Kα radiation

RSC Advances Accepted Manuscript

source. Thermo-gravimetric analysis (TGA, Seiko Instruments TG/DTA6300) was performed on the LTO-G sample in air from 100 to 800 °C with a heating rate of 10 $^{o}C\ min^{-1}$ to determine the content of graphene. The morphologies were visualized by field emission scanning electron microscopy (FE-SEM, Zeiss Sigma), and high-resolution transmission electron microscopy (TEM, JEOL JEM-2010).

2.3 Electrochemical measurements

The anode electrode was prepared by spreading uniform slurry on a copper foil. The slurry was composed of 90 wt.% LTO-G composite and 10 wt.% polyvinylidene fluoride (PVdF), evenly dispersed in N-methyl pyrrolidinone (NMP). After drying at 80 °C for 24 h to remove the NMP, the copper foil with the active materials was punched into Φ 13 mm discs and 35 mm × 40 mm rectangles. The cathode electrode, made of commercially activated carbon (YP50F, Kuraray Chemicals), was cast on aluminum foil and punched into 35 × 40 mm rectangles. The detailed AC electrode preparation information can be found in our previous work [22, 54]. Coin cells (type: 2032) with LTO-G film as the working electrode, lithium metal as the counter electrode, Celgard 2400 (Celgard company) microporous membrane as the separator and 1 M $LiPF_6$ dissolved in a mixture of EC+DEC+DMC (1:1:1 in vol.) as the electrolyte were assembled in an argon-filled glove box (MBRAUN).

A three-electrode pouch cell, denoted as the 1+1 device, was assembled with one layer of one-side coated AC electrode ($m_{AC} = 37.18$ mg) as the cathode, one layer of one-side coated LTO-G electrode ($m_{LTO-G} = 18.77$ mg) as the anode, and a lithium metal (Φ 16 mm) as a reference electrode. The schematic structure of the

RSC Advances Accepted Manuscript

capacitor is shown in Fig. 2a, and the made-up cell is shown in Fig. 2b. Another device was also assembled, and it is shown in Fig. 2c. It had 10 pieces of double-side coated AC cathode, 10 pieces of double-side coated LTO-G anode and a 30 × 35 mm Li metal as a reference electrode. This cell was denoted as the 10+10 device, and the total masses for AC, LTO-G and the whole device were 0.97, 0.47 and 10 g, respectively. The mass ratios (*r*, defined by $r = m_{AC}/m_{LTO-G}$) of both capacitors were set to be approximately 2, and the real *r* are 1.98 and 2.06 for the 1+1 and the 10+10 device, respectively.

The lithium metal electrode was used for the detection of the electrode voltage profile during the charge/discharge process, for the pre-cycling for the AC and LTO-G composite, and also for the pre-lithiation process for LTO-G anode. The electrochemical properties of the LTO-G composite and the LICs were studied by the galvanostatic charge/discharge technique between 1.0 to 2.5 V using LAND CT2001A battery testers and an Arbin MSTAT 4 multichannel galvanostat/potentiostat.

3、Results and discussion

Fig. 3 shows the XRD patterns of the LTO-G composite prepared by different method. For method I, because no real LTO-G composite was formed before the test, the XRD of the pure LTO powders was presented instead. In the XRD patterns, no diffraction peaks related to GO or graphene were detected because the GO and graphene were well dispersed in the p-LTO/GO and LTO-G and appeared to be amorphous [31, 32, 46]. The three XRD patterns in Fig. 3a are almost the same. Only the

RSC Advances Accepted Manuscript

$Li_4Ti_5O_{12}$ phase was detected, but with a different background intensity and full-width-half-maximum (FWHM). The samples containing graphene show higher background intensity, especially at a low θ range, 10-30 ^{o}. This contrast is reasonable because the graphene was amorphous and well distributed. LTO-G prepared by the two-step method shows the biggest FWHM, according to the Scherrer equation, it has the smallest mean crystalline size, which means that the two-step method could help to reduce the particle size of LTO-G. Fig. 3b shows the XRD patterns of p-LTO, p-LTO/GO and LTO-G. The p-LTO and p-LTO/GO exhibit main phase structures of spinel $Li_4Ti_5O_{12}$ oxide and rutile TiO_2 oxide. A certain amount of LiOH also was detected, which further reacted with TiO_2 to form the spinel LTO when the calcined temperature was increased to 800 ^{o}C, as shown in Fig. 3b. A single spinel structure was detected (Fig. 3b) after the p-LTO/GO was in-situ reduced in an Ar flow atmosphere at 800 ^{o}C for 2 h.

Fig. 4c and d show the morphology of the LTO-G composite prepared by the two-step method. As a comparison, the morphology of LTO-G composite prepared by method II also was presented, shown in Fig. 4a and b. The powders prepared by two-step method were smaller in size and slighter in aggregation.

The SEM images (Fig. 4c and e) indicate that the LTO powders and the graphene sheets were uniformly distributed, and the graphene sheets were well connected with each other. The uniformly-distributed and well-connected of graphene morphology provide the good conductivity of the LTO-G composite, which was further proved by the low electrode polarization during the charge/discharge

RSC Advances Accepted Manuscript

process. The TEM image (Fig. 4f) shows the detail morphology of the LTO-G composite. The LTO particles were about 200 nm in size, and the very thin and curved graphene sheets were microns in length. A regular lattice spacing of 0.48 nm was observed by HR-TEM (inset graph in Fig. 4f), which matches well with the (111) planes of spinel LTO oxide.

In order to determine the content of graphene, TG-DTA analysis was performed on the LTO-G composites, and the result is shown in Fig. 5. For the LTO-G prepared by method II, the TG curve shows that there was an 8.9% weight loss during the heating process, between 350-500 ^{o}C. For the LTO-G prepared by the two-step method, a 10.7% weight loss was detected, and this loss occurred mainly between 450-520 ^{o}C. LTO-G prepared by two-step method shows a higher exothermic peak temperature, indicating that the adhesion between LTO particles and graphene sheets was stronger than that of LTO-G prepared by method II. The strong adhesion between LTO particles and graphene sheets promoted the migration of electrons and thus produced better electronic conductivity. No other endo/exothermic peaks or weight loss processes were found in both TG-DTA curves, combining with the XRD data shown in Fig. 3, indicating that a pure LTO-G composite was synthesized.

Galvanostatic charge/discharge cycling measurement was performed to study the electrochemical performance of the LTO-G composite, and the results are shown in Fig. 6. Fig. 6a shows the comparison of the rate-capability performance of the LTO-G composite prepared by a different method. Due to the smaller size and slighter aggregation, the LTO-G composite synthesized by the two-step method

RSC Advances Accepted Manuscript

shows a higher reversible capacity and better capacity retention (inset table in Fig. 6a).

At a low charge/discharge current density, 0.1 C, (1 C = 175 mA g^{-1}), an average reversible capacity of 194, and 187 mAh g^{-1} (based on the total mass of the LTO-G) was achieved for LTO-G prepared by the two-step method and method II, respectively, as shown in Fig. 6a and b. The result was much higher than the theoretical capacity of the LTO, which may be due to the high specific capacity of graphene [4, 32, 46]. And because the graphene content in the LTO-G prepared by the two-step method was a little higher than that of method II, it is reasonable that LTO-G prepared by two-step method could deliver higher reversible capacity, as shown in Fig. 6a. With the increase of charge/discharge current density, the reversible capacity slowly decreased. And the specific capacity restored to 190 mAh g^{-1} when the charge/discharge rate was changed back from 28.6 C to 0.1 C, which suggests that the LTO-G composite shows very good capacity recovery due to the having good intrinsic structure stability of the LTO material [28]. Specific capacities of 180, 178, 174, 164, 150, 127 and 90 mAh g^{-1} were achieved for 0.3, 0.6, 1.1, 2.9, 5.7, 11.4 and 28.6 C respectively.

The galvanostatic curves at different rates are shown in Fig. 6c. An exclusive flat potential plateau about 1.44~1.71 V (vs. Li^+/Li) was found at all rates, which corresponds well to the two phase equilibrium between $Li_4Ti_5O_{12}$ and $Li_7Ti_5O_{12}$ [33, 34]. With the increase of current density, the discharge voltage plateau of the LTO-G composite shifts gradually toward low voltage, and the charge voltage plateau shifts

RSC Advances Accepted Manuscript

gradually toward high voltage, showing the electrode polarization at high current density. The corresponding electrode polarization (ΔE) between charge/discharge curves as a function of the current density is plotted in Fig. 6d. Very small electrode polarization, 0.027 V at 0.1 C, 0.043 V at 0.3 C, 0.051 V at 0.6 C, 0.077 V at 1.1 C, was observed, suggesting that the LTO-G composite exhibits very good conductivity. Because no conductive additive was used in the working electrode, we conclude that the good conductivity was the intrinsic property of LTO-G composite.

Fig. 6e and f show the cycling performance of the LTO-G composite at 1.1 C and 5.7 C respectively. At 1.1 C, LTO-G composite delivered a charge capacity of 176 mAh g^{-1} during the first cycle, which agrees well with the result of the rate-capacity test (Fig. 6b); the capacity gradually decreased to 167 mAh g^{-1} at the 100^{th} cycle (Fig. 6e). At the higher charge/discharge rate, 5.7 C, the material delivered 150 mAh g^{-1} during the first cycle, but decreased rapidly after the completion of the first 100 cycles (132 mAh g^{-1} at 100^{th} cycle, 88% capacity retention), and the capacity decreased very slowly thereafter. After 2000 cycles, it still delivered a capacity of 120 mAh g^{-1} (80% capacity retention), which indicates that the LTO-G composite shows excellent Li^+ insertion/extraction kinetic properties.

Two three-electrode pouch capacitors, as shown in Fig. 2, were assembled and studied. Before the electrochemical cycling test was performed, the AC cathode was pre-cycled between 2.0 and 4.2 V at a current density of 5 mA g^{-1} for 4 cycles, and the LTO-G electrode was pre-lithiated, The results are presented in Fig. 7. The AC potential was linearly proportional to the charge/discharge time, and the capacity was

RSC Advances Accepted Manuscript

calculated to be 64 mAh g^{-1} between 2.0-4.2 V, as shown in Fig. 7a. The pre-lithiation process of LTO-G was performed to make the LTO-G anode work at the Li^+ insertion/extraction voltage platform, as shown in the specific capacity-voltage profiles (Fig. 6c). The voltage profile of the pre-lithiation process is shown in Fig. 7b. For the 1+1 device, a current of 1 mA (equal to 0.3 C) was applied between the LTO-G and Li-metal electrode for 33.8 min (the pre-lithiation capacity was calculated to be 30 mAh g^{-1}). Since the Li-metal was placed against the LTO-G electrode (shown in Fig. 2a), it was difficult for Li^+ to transfer from Li-metal to LTO, and therefore a much higher electrode polarization was detected. The voltage platform was 1.25 V, much lower than the voltage platform shown in Fig. 4c (1.54 V at 0.6 C). When the LTO-G electrode was discharged at 30 mAh g^{-1}, the charge was removed, and the voltage of 1.55 V was detected between the LTO-G anode and the Li-metal electrode, indicating that there was a two phase equilibrium between $Li_4Ti_5O_{12}$ and $Li_7Ti_5O_{12}$ [33, 34]. For the 10+10 device, the Li^+ migration is more difficult in the pre-lithiation process, and a much smaller current density of 0.05 C was used (Fig. 8). No obvious voltage platform was detected during the pre-lithiation process. Because the mass ratio of cathode to anode for the 10+10 device ($r_{10|10} = 2.06$) was a little higher than that of the 1+1 device ($r_{1|1} = 1.98$), a higher pre-lithiathion cut-off capacity (35 mAh g^{-1}) was applied for the 10+10 device, as shown in the inset table in Fig. 7b.

Fig. 8 shows the electrochemical performance of the AC/LTO-G Li-ion hybrid capacitor cycling at different current densities. The 1+1 device was first cycled at a

RSC Advances Accepted Manuscript

current density of 0.1 C, and the results are shown in Fig. 8a. The inset graph in Fig. 9a shows the potential profile of the first 4 cycles. The cathode potential was linearly proportional to the charge/discharge time, varying from 2.58 to 3.99 V vs. Li/Li^+, indicating the typical electrical double layer capacitor behavior. A flat potential signal, about 1.50 V vs. Li/Li^+, was detected at the anode, which corresponds to the two phase equilibrium between $Li_4Ti_5O_{12}$ and $Li_7Ti_5O_{12}$ [33, 34], indicating the typical charge/discharge behavior of LTO material. According to the pre-cycling result of the AC electrode (Fig. 7), the capacity of AC at the potential range of 2.58 and 3.99 V was about 41 mAh g^{-1}. The mass ratio r = 1.98, the capacity of the cell (based on AC) was calculated to be 81 mAh g^{-1}, which agrees well with the result based on the LTO-G listed in Fig. 8a. The result indicates that only about 45% of the LTO-G was utilized, so the capacity can be further increased by increasing the mass ratio of the cathode to the anode.

Fig. 8b shows the rate-capability performance of the AC/LTO-G Li-ion hybrid capacitors. For the 1+1 device, averages of 75, 70, 67, 62, 56, 48 and 37 were achieved for 0.5, 1, 2, 5, 10, 20, and 50 C, respectively. For the 10+10 device, the specific capacity was a little smaller than that of the 1+1 device. The average capabilities of 71, 67, 65, 61, 55, 45, and 30 were achieved for 0.5, 1, 2, 5, 10, 20, and 50 C, respectively.

The energy densities based on the total mass of the active material of these two devices are almost the same: about 50 Wh kg^{-1} at 10 W kg^{-1} (cycled at 0.1 C), 30 Wh kg^{-1} at 1000 W kg^{-1} (at 10 C) and 15 Wh kg^{-1} at 4000 W kg^{-1} (at 50 C), as shown in

RSC Advances Accepted Manuscript

the Fig. 8c. The AC/LTO-G Li-ion hybrid capacitors were then charged and discharged at 10 C for 10,000 cycles, and the result is shown in Fig. 8d. The 1+1 device delivered a capacity of 57 mAh g^{-1} (32 Wh kg^{-1}) during the first cycle, and then slowly decreased to 47 mAh g^{-1} (26 Wh kg^{-1}, 81% capacity retention). The 10+10 device delivered 56 mAh g^{-1} (32 Wh kg^{-1}) during the first cycle but decreased quickly to 45 mAh g^{-1} (25 Wh kg^{-1}, 80% capacity retention) by the 500^{th} cycle, and remained at 40 mAh g^{-1} (22 Wh kg^{-1}, 71% capacity retention) after 10,000 cycles. The highest energy density based on the total mass of the 10+10 device was 6.6 Wh kg^{-1}, and it can be further increased by increasing the mass ratio of the cathode to the anode. The total active material accounted for only 15% of the whole device, still leaving much room for improvement in energy density, which indicates that the LTO-G composite is a promising candidate material for Li-ion hybrid capacitors.

4、Conclusion

$Li_4Ti_5O_{12}$-graphene (LTO-G) was successfully synthesized by a two-step method. The two-step method prepared LTO-G was first heat-treated at a low temperature, and thus can produce finer p-LTO powders. The resulting GO coating layer prevents the p-LTO powders from aggregation and thus prevents the particle size of the LTO from increasing during the further heat treatment at 800 ^oC. The two-step method also provides stronger adhesion between LTO particles and graphene sheets, and thus produces LTO-G composite with good conductivity. Coupled with Li metal as a lithium ion half-cell, the LTO-G anode shows a high specific capacity. 194, 178, 150, 127, 90 mAh g^{-1} were achieved for 0.1, 0.6, 5.7,

RSC Advances Accepted Manuscript

11.4, 28.6 C, respectively. The potential profile of the capacitor shows a typical double layer capacitor behavior of AC and a typical charge/discharge behavior of LTO material, indicating that the li-ion hybrid capacitor-performed successfully. The 1+1 device delivers 80 mAh g^{-1} at 0.1 C, very close to the theoretical capacity of a capacitor with $r = 2$. The energy densities are 30 Wh kg^{-1} at 1000 W kg^{-1} and 15 Wh kg^{-1} at 4000 W kg^{-1}, and after 10,000 cycles, the capacitors still deliver an energy density higher than 22 Wh kg^{-1}. The highest energy density based on the total mass of the whole device is 6.6 Wh kg^{-1}, which leaves much room for improvement.

Acknowledgements

This work was financially supported by the China Postdoctoral Science Foundation funded project (No. 2014M550087) and National Natural Science Foundation of China (No. 51307167 and 51472238).

RSC Advances Accepted Manuscript

Figure captions

Figure 1. Schematic presentation of the synthetic process of the LTO-G composite.

Figure 2. (a) Schematic structure of the three-electrode lithium-ion hybrid capacitor; (b) the make-up of the soft-packaged 1+1 device; (c) the make-up of soft-packaged 10+10 device.

Figure 3. XRD patterns of (a) LTO-G composite prepared by different methods and (b) p-LTO, p-LTO/GO and LTO-G materials.

Figure 4. Morphology of the LTO-G composite. (a, b) SEM images of LTO-G prepared by method II; (c-e) SEM images of LTO-G prepared by the two-step method; (f) TEM image of LTO-G prepared by the two-step method (inset graph: HR-TEM micrograph)

Figure 5. TG-DTA curves of LTO-G composites prepared by different method.

Figure 6. Electrochemical performance for the LTO-G composite. (a) rate-capacity performance of LTO-G composite prepared by different method (inset table: capacity retention at different charge/discharge current density); (b) rate-capability; (c) specific capacity-voltage profiles; (d) polarization of ΔE at different charge/discharge current density; (e) cycling performance at 200 mA g^{-1} (1.1 C); (f) cycling performance at 1 A g^{-1} (5.7 C)

Figure 7. Potential profile of (a) pre-cycling of the AC electrode and (b) pre-lithiation process of the LTO-G electrode.

Figure 8. Electrochemical performances of the AC/LTO-G Li-ion hybrid capacitor. (a) cycling performance at 0.1 C (inset graph: the potential profile of first 4 cycles); (b) rate-capability; (c) ragone plots (inset graph: schematic structure of the

RSC Advances Accepted Manuscript

three-electrode lithium-ion hybrid capacitor); (d) cycling performance at 10 C

RSC Advances Accepted Manuscript

References

1. M. D. Stoller, S. Murali, N. Quarles, Y. Zhu, J. R. Potts, X. Zhu, H. W. Ha and R. S. Ruoff, *Physical Chemistry Chemical Physics*, 2012, **14**, 3388-3391.
2. A. Jain, V. Aravindan, S. Jayaraman, P. S. Kumar, R. Balasubramanian, S. Ramakrishna, S. Madhavi and M. P. Srinivasan, *Scientific reports*, 2013, **3**, 3002.
3. S. R. Sivakkumar and A. G. Pandolfo, *Electrochimica Acta*, 2012, **65**, 280-287.
4. K. Leng, F. Zhang, L. Zhang, T. Zhang, Y. Wu, Y. Lu, Y. Huang and Y. Chen, *Nano Research*, 2013, **6**, 581-592.
5. K. Naoi, S. Ishimoto, Y. Isobe and S. Aoyagi, *Journal of Power Sources*, 2010, **195**, 6250-6254.
6. A. Vlad, N. Singh, J. Rolland, S. Melinte, P. M. Ajayan and J. F. Gohy, *Scientific reports*, 2014, **4**, 4315.
7. D. Puthusseri, V. Aravindan, S. Madhavi and S. Ogale, *Electrochimica Acta*, 2014, **130**, 766-770.
8. W. J. Cao and J. P. Zheng, *Journal of Power Sources*, 2012, **213**, 180-185.
9. A. Brandt and A. Balducci, *Electrochimica Acta*, 2013, **108**, 219-225.
10. H. Kim, M. Y. Cho, M. H. Kim, K. Y. Park, H. Gwon, Y. Lee, K. C. Roh and K. Kang, *Advanced Energy Materials*, 2013, **3**, 1500-1506.
11. C. Liu, Z. Yu, D. Neff, A. Zhamu and B. Z. Jang, *Nano letters*, 2010, **10**, 4863-4868.

RSC Advances Accepted Manuscript

12. X. Hu, Y. Huai, Z. Lin, J. Suo and Z. Deng, *Journal of The Electrochemical Society*, 2007, **154**, A1026.

13. N. Böckenfeld, R. S. Kühnel, S. Passerini, M. Winter and A. Balducci, *Journal of Power Sources*, 2011, **196**, 4136-4142.

14. H. Wu, C. V. Rao and B. Rambabu, *Materials Chemistry and Physics*, 2009, **116**, 532-535.

15. A. Du Pasquier, I. Plitz, S. Menocal and G. Amatucci, *Journal of Power Sources*, 2003, **115**, 171-178.

16. W.H. Qu, F. Han, A.H. Lu, C. Xing, M. Qiao and W.C. Li, *Journal of Materials Chemistry A*, 2014, **2**, 6549-6557.

17. K. Naoi, S. Ishimoto, J. i. Miyamoto and W. Naoi, *Energy & Environmental Science*, 2012, **5**, 9363.

18. S. W. Lee, B. M. Gallant, H. R. Byon, P. T. Hammond and Y. Shao Horn, *Energy & Environmental Science*, 2011, **4**, 1972.

19. H. Wang and M. Yoshio, *Electrochemistry Communications*, 2008, **10**, 382-386.

20. X. Yu, C. Zhan, R. Lv, Y. Bai, Y. Lin, Z.H. Huang, W. Shen, X. Qiu and F. Kang, *Nano Energy*, 2015, **15**, 43-53.

21. S. Kumagai, T. Ishikawa and N. Sawa, *Journal of Energy Storage*, 2015, **2**, 1-7.

22. X. Sun, X. Zhang, H. Zhang, N. Xu, K. Wang and Y. Ma, *Journal of Power Sources*, 2014, **270**, 318-325.

RSC Advances Accepted Manuscript

23. J. J. Yang, C. H. Choi, H. B. Seo, H. J. Kim and S. G. Park, *Electrochimica Acta*, 2012, **86**, 277-281.

24. H. G. Jung, N. Venugopal, B. Scrosati and Y.K. Sun, *Journal of Power Sources*, 2013, **221**, 266-271.

25. L. Cheng, H. J. Liu, J. J. Zhang, H. M. Xiong and Y. Y. Xia, *Journal of The Electrochemical Society*, 2006, **153**, A1472.

26. L. Ye, Q. Liang, Y. Lei, X. Yu, C. Han, W. Shen, Z.H. Huang, F. Kang and Q.H. Yang, *Journal of Power Sources*, 2015, **282**, 174-178.

27. S. Dsoke, B. Fuchs, E. Gucciardi and M. Wohlfahrt-Mehrens, *Journal of Power Sources*, 2015, **282**, 385-393.

28. J. Wang, H. Zhao, Y. Wen, J. Xie, Q. Xia, T. Zhang, Z. Zeng and X. Du, *Electrochimica Acta*, 2013, **113**, 679-685.

29. C. He, S. Wu, N. Zhao, C. Shi, E. Liu and J. Li, *ACS Nano*, 2013, **7**, 4459-4469.

30. P. Poizot, S. Laruelle, S. Grugeon, L. Dupont and J. M. Tarascon, *Nature*, 2000, **407**, 496-499.

31. Q. H. Wu, C. Wang and J. G. Ren, *Ionics*, 2013, **19**, 1875-1882.

32. Y. Shi, L. Wen, F. Li and H. M. Cheng, *Journal of Power Sources*, 2011, **196**, 8610-8617.

33. K. S. Park, A. Benayad, D. J. Kang and S. G. Doo, *Journal of the American Chemical Society*, 2008, **130**, 14930-14931.

34. Y. Wang, H. Liu, K. Wang, H. Eiji, Y. Wang and H. Zhou, *Journal of*

RSC Advances Accepted Manuscript

Materials Chemistry, 2009, **19**, 6789-6795.

35. G. N. Zhu, H. J. Liu, J. H. Zhuang, C. X. Wang, Y. G. Wang and Y. Y. Xia, *Energy & Environmental Science*, 2011, **4**, 4016-4022.

36. J. Lim, E. Choi, V. Mathew, D. Kim, D. Ahn, J. Gim, S. H. Kang and J. Kim, *Journal of The Electrochemical Society*, 2011, **158**, A275.

37. S. G. Ri, L. Zhan, Y. Wang, L. Zhou, J. Hu and H. Liu, *Electrochimica Acta*, 2013, **109**, 389-394.

38. A. S. Prakash, P. Manikandan, K. Ramesha, M. Sathiya, J. M. Tarascon and A. K. Shukla, *Chemistry of Materials*, 2010, **22**, 2857-2863.

39. L. Cheng, J. Yan, G. N. Zhu, J. Y. Luo, C. X. Wang and Y. Y. Xia, *Journal of Materials Chemistry*, 2010, **20**, 595.

40. E. Kang, Y. S. Jung, G. H. Kim, J. Chun, U. Wiesner, A. C. Dillon, J. K. Kim and J. Lee, *Advanced Functional Materials*, 2011, **21**, 4349-4357.

41. N. Zhu, W. Liu, M. Xue, Z. Xie, D. Zhao, M. Zhang, J. Chen and T. Cao, *Electrochimica Acta*, 2010, **55**, 5813-5818.

42. J. Huang and Z. Jiang, *Electrochimica Acta*, 2008, **53**, 7756-7759.

43. A. K. GEIM and K. S. NOVOSELOV, *nature materials*, 2007, **6**, 183-191.

44. S. M. Paek, E. Yoo and I. Honma, *Nano letters*, 2009, **9**, 72-75.

45. E. Yoo, J. Kim, E. Hosono, H. s. Zhou, T. Kudo and I. Honma, *Nano letters*, 2008, **8**, 2277-2282.

46. D. Pan, S. Wang, B. Zhao, M. Wu, H. Zhang, Y. Wang and Z. Jiao, *Chemistry of Materials*, 2009, **21**, 3136-3142.

RSC Advances Accepted Manuscript

47. L. Zhang, F. Zhang, X. Yang, G. Long, Y. Wu, T. Zhang, K. Leng, Y. Huang, Y. Ma, A. Yu and Y. Chen, *Scientific reports*, 2013, **3**, 1408.

48. Y. Huang, J. Liang and Y. Chen, *Small*, 2012, **8**, 1805-1834.

49. X. Zhang, H. Zhang, C. Li, K. Wang, X. Sun and Y. Ma, *RSC Advances*, 2014, **4**, 45862-45884.

50. Y. Zhu, S. Murali, W. Cai, X. Li, J. W. Suk, J. R. Potts and R. S. Ruoff, *Advanced materials*, 2010, **22**, 3906-3924.

51. K. S. Novoselov, V. I. Fal'ko, L. Colombo, P. R. Gellert, M. G. Schwab and K. Kim, *Nature*, 2012, **490**, 192-200.

52. M. D. Stoller, S. Park, Y. Zhu, J. An and R. S. Ruoff, *Nano letters*, 2008, **8**, 3498-3502.

53. L. L. Zhang, R. Zhou and X. S. Zhao, *Journal of Materials Chemistry*, 2010, **20**, 5983.

54. X. Sun, X. Zhang, B. Huang, H. Zhang, D. Zhang and Y. Ma, *Journal of Power Sources*, 2013, **243**, 361-368.

RSC Advances Accepted Manuscript

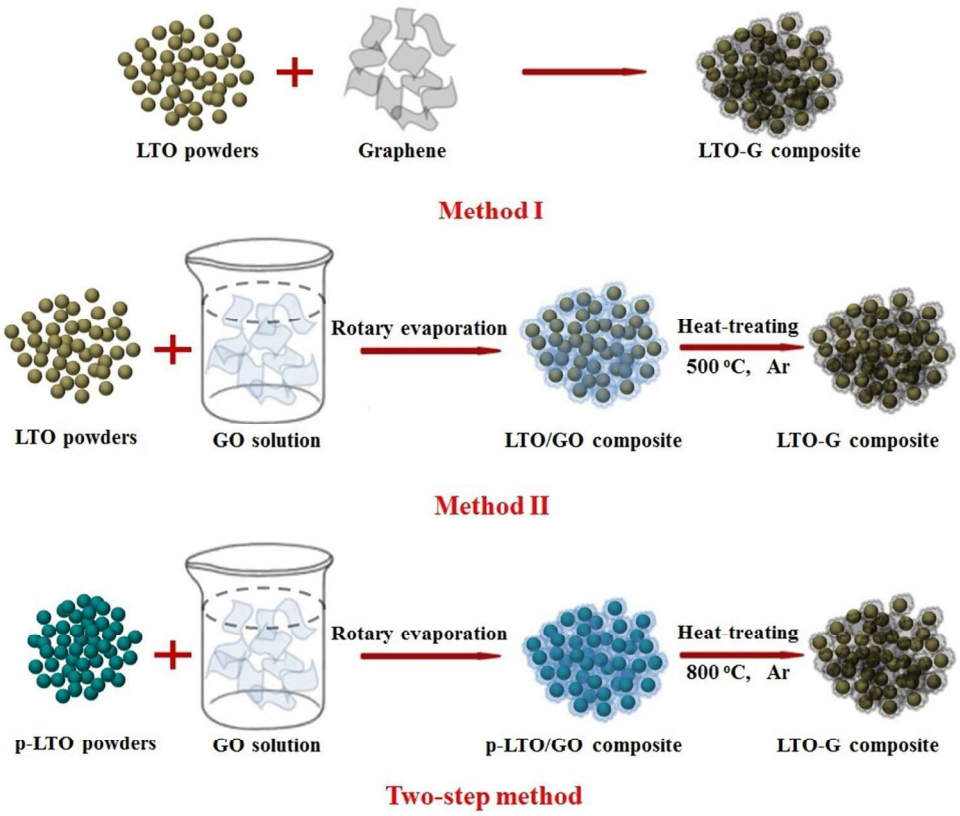

Figure 1. Schematic presentation of the synthetic process of the LTO-G composite.
352x295mm (72 x 72 DPI)

RSC Advances Accepted Manuscript

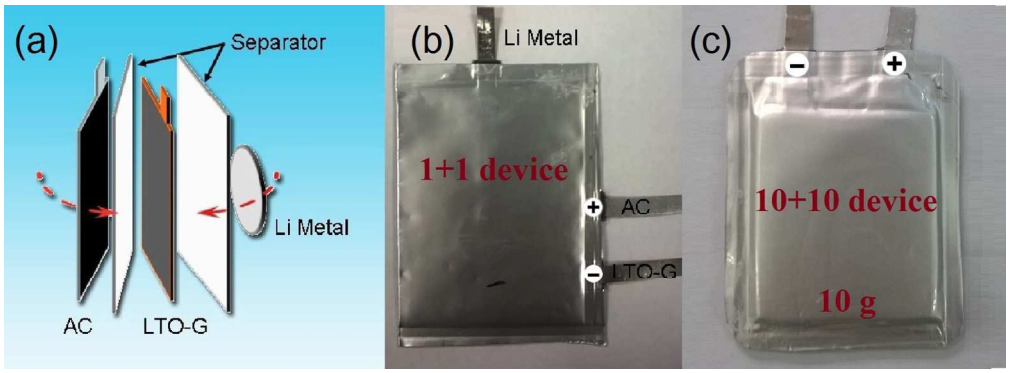

Figure 2. (a) Schematic structure of the three-electrode lithium-ion hybrid capacitor; (b) the make-up of the soft-packaged 1+1 device; (c) the make-up of soft-packaged 10+10 device.
271x98mm (150 x 150 DPI)

RSC Advances Accepted Manuscript

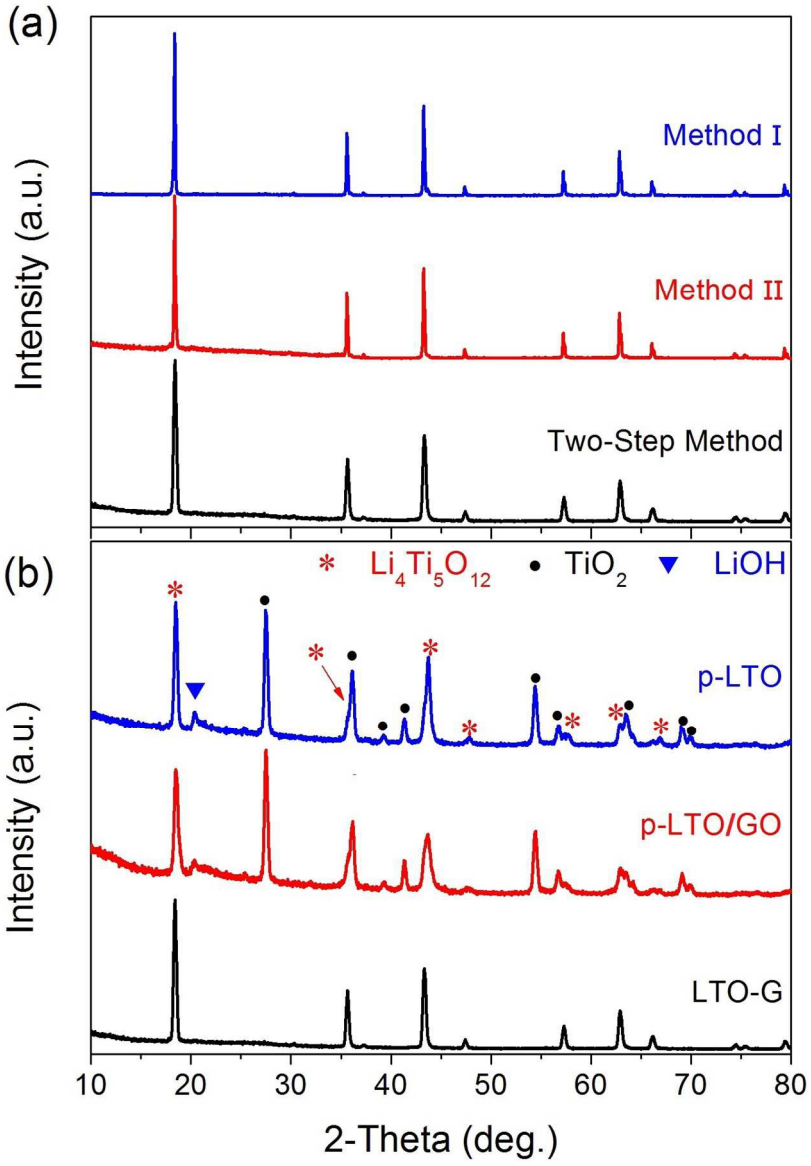

Figure 3. XRD patterns of (a) LTO-G composite prepared by different methods and (b) p-LTO, p-LTO/GO and LTO-G materials.
252x337mm (150 x 150 DPI)

RSC Advances Accepted Manuscript

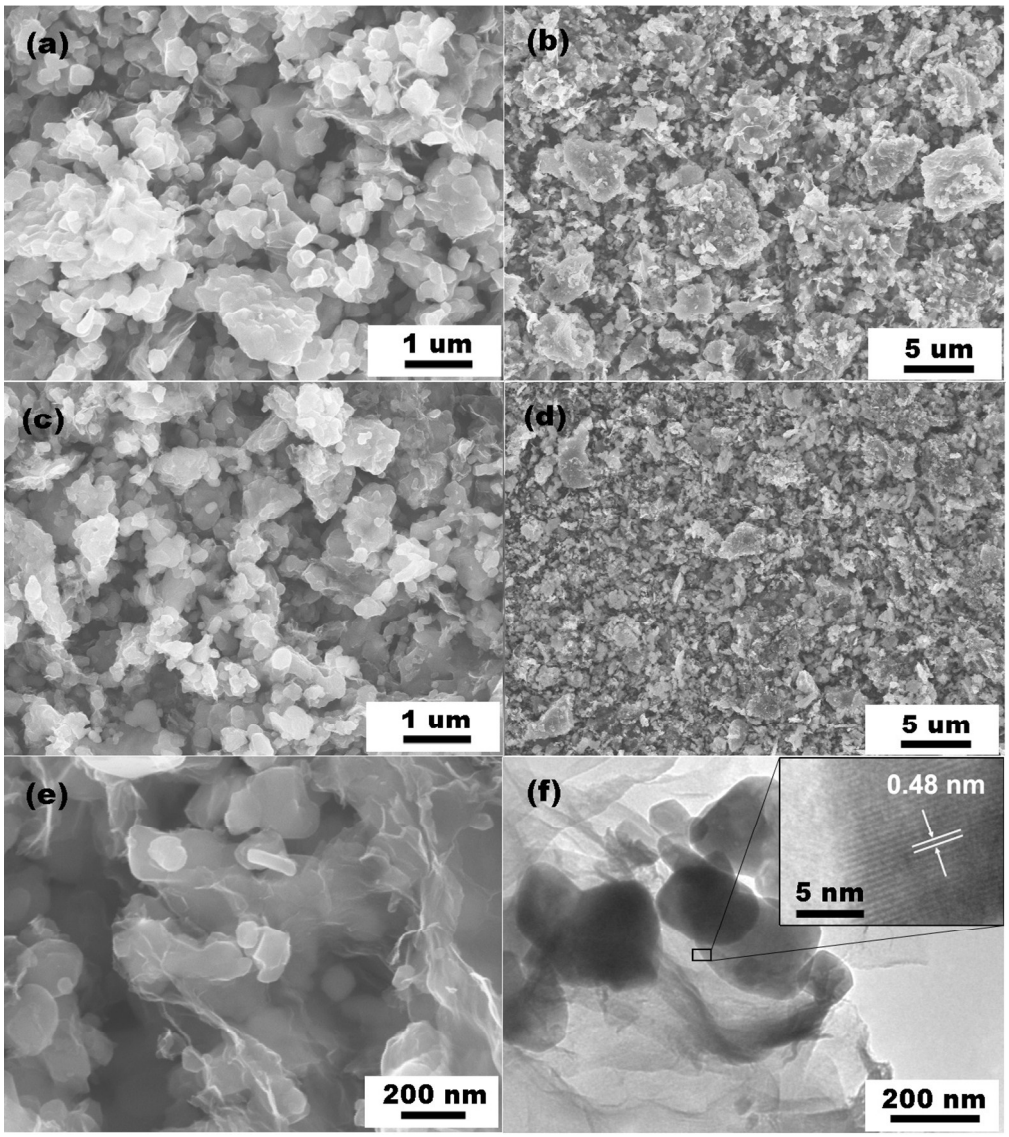

Figure 4. Morphology of the LTO-G composite. (a, b) SEM images of LTO-G prepared by method II; (c-e) SEM images of LTO-G prepared by the two-step method; (f) TEM image of LTO-G prepared by the two-step method (inset graph: HR-TEM micrograph)
478x540mm (72 x 72 DPI)

RSC Advances Accepted Manuscript

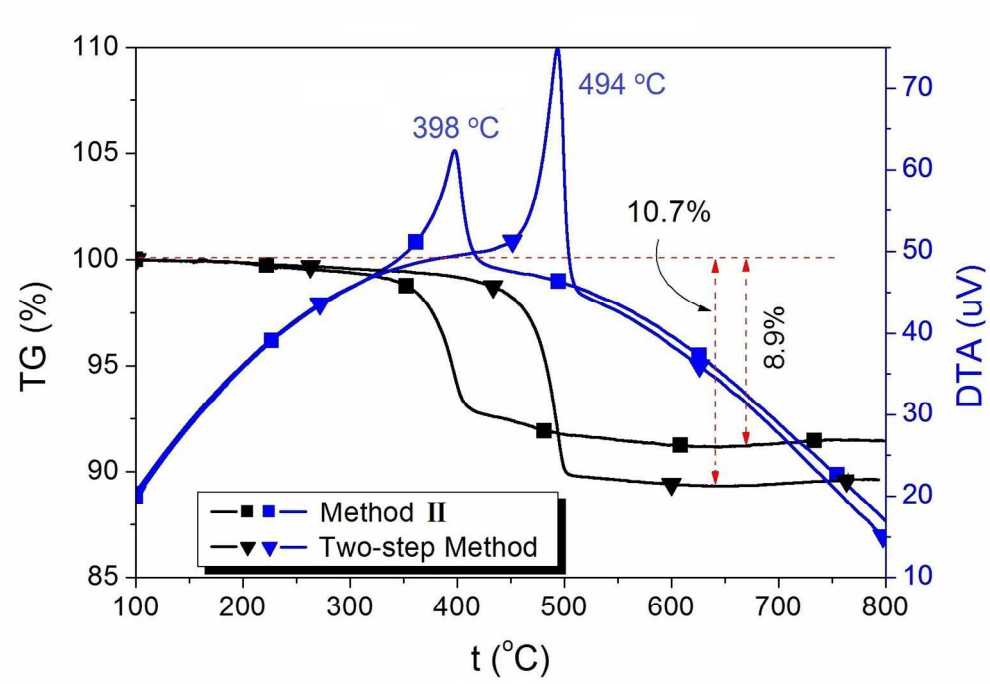

Figure 5. TG-DTA curves of LTO-G composites prepared by different method.
297x209mm (150 x 150 DPI)

RSC Advances Accepted Manuscript

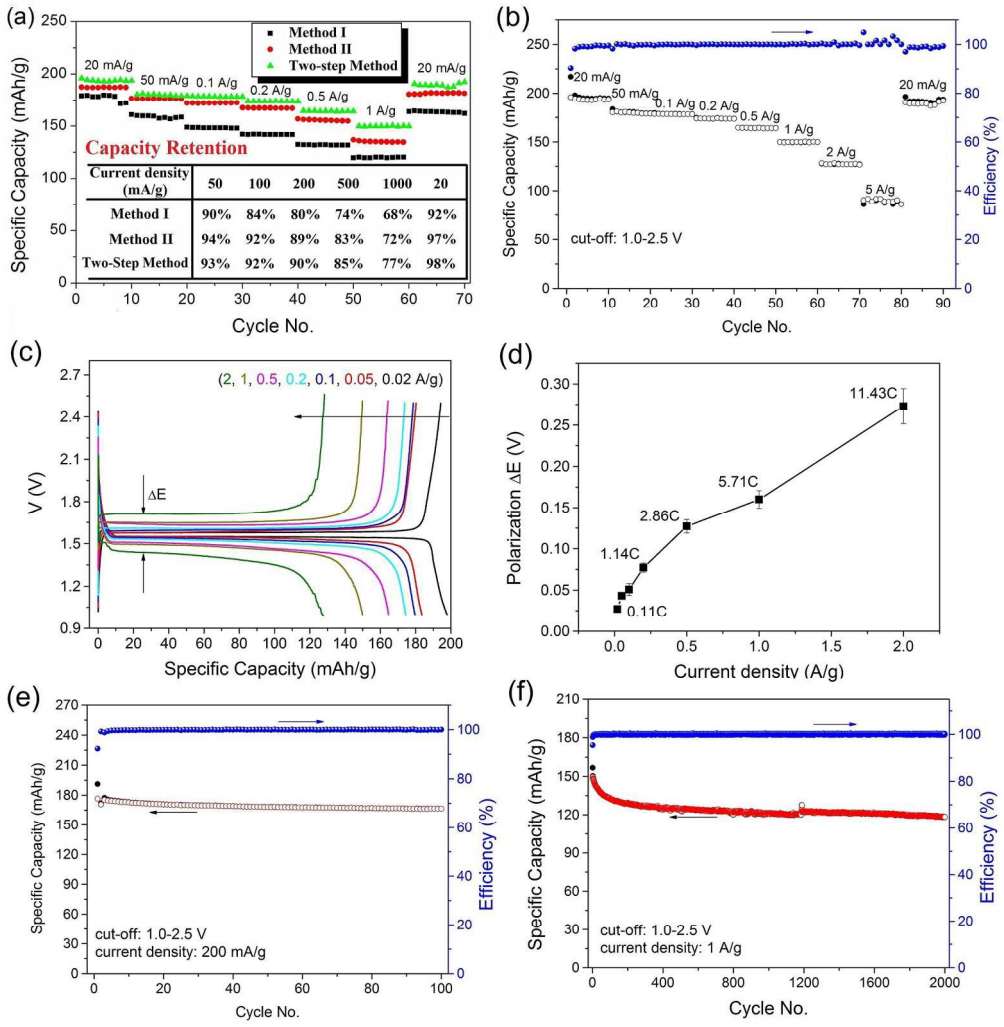

Figure 6. Electrochemical performance for the LTO-G composite. (a) rate-capacity performance of LTO-G composite prepared by different method (inset table: capacity retention at different charge/discharge current density); (b) rate-capability; (c) specific capacity-voltage profiles; (d) polarization of ΔE at different charge/discharge current density; (e) cycling performance at 200 mA g-1 (1.1 C); (f) cycling performance at 1 A g-1 (5.7 C)
359x369mm (150 x 150 DPI)

RSC Advances Accepted Manuscript

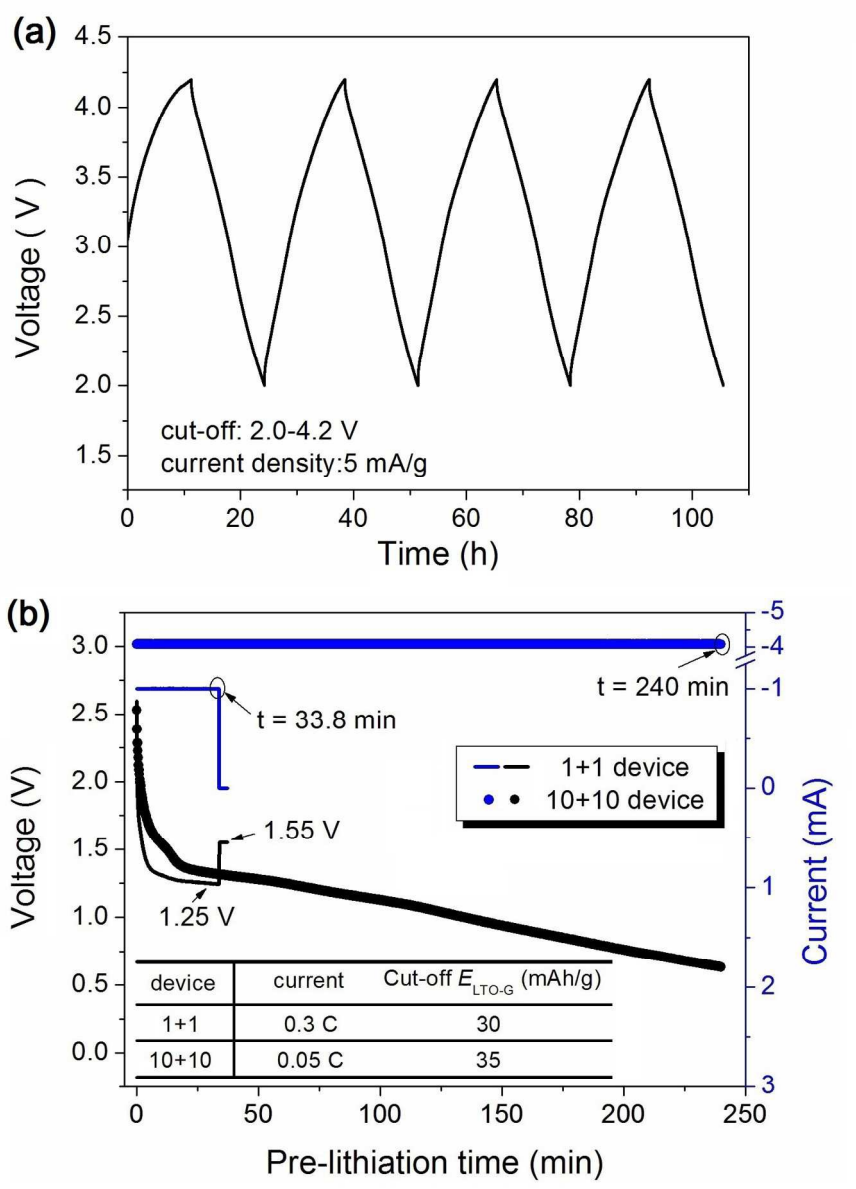

Figure 7. Potential profile of (a) pre-cycling of the AC electrode and (b) pre-lithiation process of the LTO-G electrode.
276x380mm (150 x 150 DPI)

RSC Advances Accepted Manuscript

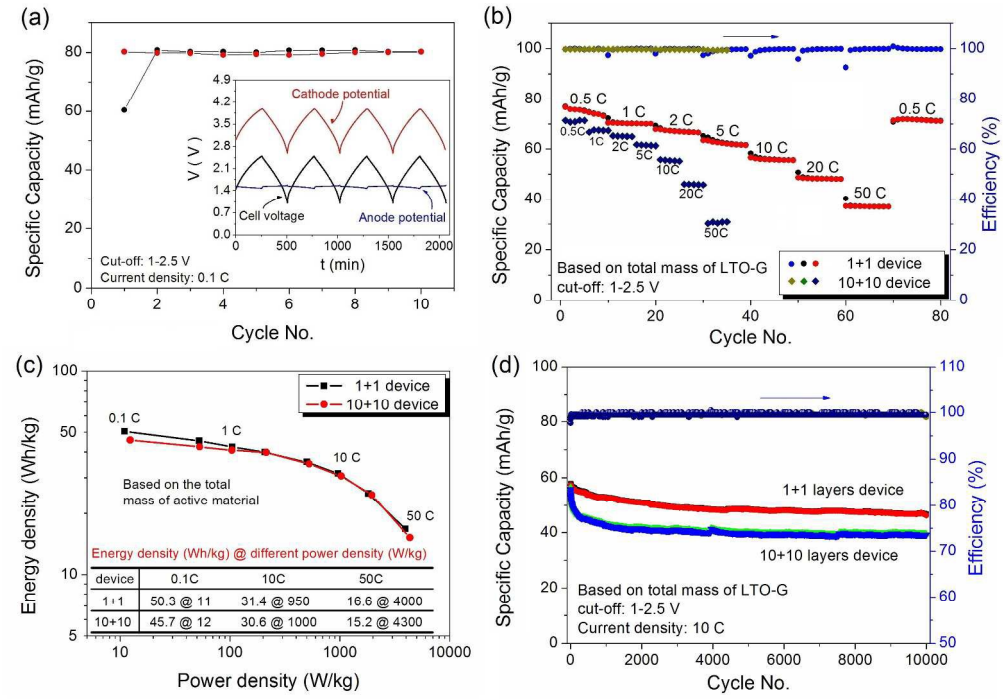

Figure 8. Electrochemical performances of the AC/LTO-G Li-ion hybrid capacitor. (a) cycling performance at 0.1 C (inset graph: the potential profile of first 4 cycles); (b) rate-capability; (c) ragone plots (inset graph: schematic structure of the three-electrode lithium-ion hybrid capacitor); (d) cycling performance at 10 C
543x381mm (150 x 150 DPI)

RSC Advances Accepted Manuscript